

Extremum Seeking Controlled Wiggling for Tactile Insertion

Levi Burner^{1*}, Pavan Mantripragada^{2*}, Gabriele M. Caddeo^{3,4}, Lorenzo Natale³,
Cornelia Fermüller⁵, Yiannis Aloimonos^{2,5}

Abstract—When humans perform insertion tasks such as inserting a cup into a cupboard, routing a cable, or key insertion, they wiggle the object and observe the process through tactile and proprioceptive feedback. While recent advances in tactile sensors have resulted in tactile-based approaches, there has not been a generalized formulation based on wiggling similar to human behavior. Thus, we propose an extremum-seeking control law that can insert four keys into four types of locks without control parameter tuning despite significant variation in lock type. The resulting model-free formulation wiggles the end effector pose to maximize insertion depth while minimizing strain as measured by a GelSight Mini tactile sensor that grasps a key. The algorithm achieves a 71% success rate over 120 randomly initialized trials with uncertainty in both translation and orientation. Over 240 deterministically initialized trials, where only one translation or rotation parameter is perturbed, 84% of trials succeeded. Given tactile feedback at 13 Hz, the mean insertion time for these groups of trials are 262 and 147 seconds respectively.

I. INTRODUCTION

Imagine inserting a cup into a crowded cupboard. There are many objects in the way of where you want to put the cup, but somehow as the cup is inserted, they are pushed aside and the cup is placed in the appropriate location. A similar process occurs when routing a cable through a hole or inserting a key into a lock. We call such insertion problems crowded, through, and direct, respectively, and note that humans can accomplish all of them from a young age but robots still struggle. Further, general-purpose robots will need to solve such problems frequently.

During such insertion tasks, humans often wiggle the object to be inserted as a strategy to increase insertion depth. Further, tactile feedback from the fingers provides both a source of compliance and a strain measurement due to the grasped rigid object. Thus, it is interesting to study generalizable insertion algorithms that use strain-like tactile feedback and control laws based on wiggling motions. Since, in particular, general-purpose robots will need to be able to

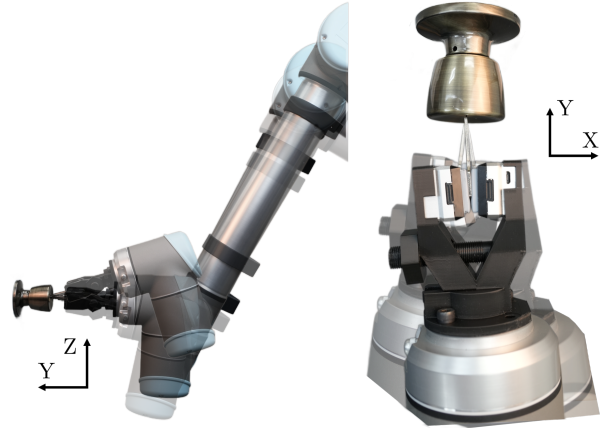


Fig. 1: By wiggling the 6 degree of freedom pose of a key grasped between two GelSight Mini tactile sensors and observing a strain-like quantity through the optical flow in the GelSight cameras, an extremum-seeking control law can insert a key into a lock. All parameters are sinusoidally modulated simultaneously but at different frequencies, allowing for the estimation of a direction that minimizes strain and maximizes insertion depth along the Y axis.

use keys to enter buildings or unlock containers, we focus on key insertion in this paper.

A compliant gripper can be realized as shown in Figure 1, where two GelSight Mini tactile sensors grasp a key between two gel pads [1]. The pads experience strain when attempting to insert a key into a lock, which can be observed through internal cameras that point toward the back of the gel.

Additionally, a control strategy based on wiggling can be realized through Extremum Seeking Control, a 100-year-old method for real-time optimization of objective functions [2]. Due to its model-free formulation, it finds application in systems that are difficult to model, such as wind turbines and solar panels (which must handle changing weather), control of particle beams, and aircraft that experience flow instability [3]. Traditionally, and in this paper, extremum seeking control laws sinusoidally perturb, or wiggle, the optimized variables and observing the effects of these perturbations by demodulating the response of the error function.

* Equal Contribution

¹ Corresponding author. Perception and Robotics Group, Electrical and Computer Engineering, University of Maryland, College Park, lburner@umd.edu

² Perception and Robotics Group, Department of Computer Science, University of Maryland, College Park, mppavan@umd.edu

³ Istituto Italiano di Tecnologia, Via San Quirico, 19 D, Genova, Italy. {gabriele.caddeo, lorenzo.natale}@iit.it

⁴ DIBRIS, Università di Genova, Via All'Opera Pia, 13, Genova, Italy.

⁵ Perception and Robotics Group, University of Maryland Institute for Advanced Computer Studies, University of Maryland, College Park {fer, jyaloimo}@umiacs.edu

Code and experimental data are available at prg.cs.umd.edu/ESTac

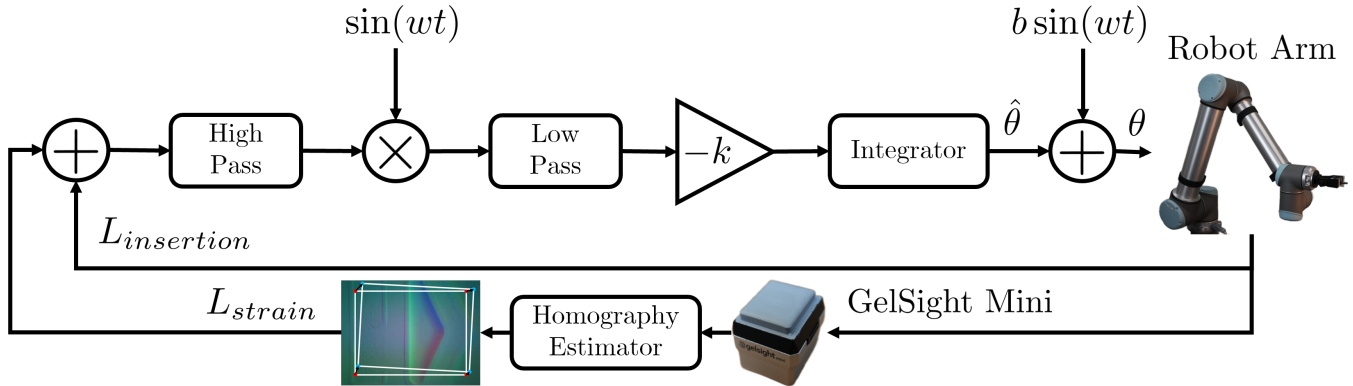


Fig. 2: The extremum seeking controlled pipeline for wiggling-based tactile insertion. The instantaneous parameters θ control the pose of the tip of a key through a UR10 robot arm. The strain that the key exerts on the GelSight Mini’s gel pad is observed via a displacement of the corners of a tracked patch in the sensor image feed, L_{strain} . The objective to be minimized is the sum of L_{strain} plus $L_{insertion}$, where $L_{insertion}$ represents the depth of insertion into the lock. The extremum seeking control seeks to minimize the objective by adjusting the parameter estimates $\hat{\theta}$. As is standard in Extremum Seeking Control, θ is a modulated version of $\hat{\theta}$ with each parameter modulated at a different frequency. The high pass filter removes the DC component from the objective signal, demodulation determines the slope of the objective’s gradient, and the low pass filter averages the feedback signal with greater high-frequency attenuation than the integrator.

When applied to tactile insertion, the proposed extremum seeking control formulation wiggles the 6 degree of freedom pose of the end-effector to minimize some objective function of tactile feedback and end-effector pose. A block diagram is given in Figure 2. This formulation is general, and future work can consider many adaptations to improve performance and address different insertion problems. In particular, we propose several “crowded,” “through,” and “direct” insertion problems that could be studied through Extremum Seeking Control and tactile feedback in Table III.

A list of our contributions follows:

- An algorithm for insertion that exploits the strategy of wiggling via model-free Extremum Seeking Control.
- Application of a direct method based on optical flow to measure strain-like forces on a GelSight Mini pad when grasping planar and rigid objects, such as keys.
- Detailed evaluation of the method of key-in-lock insertion on four locks, each with two experiments, amounting to 360 trials without any parameter tuning except for the specification of the key length.

II. RELATED WORK

Robotic key insertion has received little attention. In [4] the problem of inserting a key into a bicycle lock is considered and solved with a bimanual approach with uncertainty in lock orientation on a single axis. In [5] the problem of localization of a keyhole using an a priori determined map of key to lock contact configurations is considered. However, key insertion, and the other problems we call direct insertion problems are similar to the peg-in-hole problems considered in the field of robotics assembly. While some works also use wiggling, they do so with feedforward motions and without realtime tactile feedback [6], [7], [8]. Similarly, while Extremum Seeking Control has

found extensive application in traditional engineering fields [3], to our knowledge, it has not been used as the foundation of an algorithm for robotic insertion. The closest work is an extremum seeking control method for grasping with a gripper [9]. Existing methods for the peg-in-hole problem often focus on object and sensor specific contact modeling [10], [11] while our method does not have a contact model. Other methods consider estimating the location of the grasped object within the grasp [12], vision based feedback [13], [14], force or impedance feedback [15], [16], [17], [18], learning based approaches [19], [20], and one recent work considers adaptive finger manipulators that can passively adapt its grasp [21].

Due to the GelSight sensor’s versatile feedback in the form of images, GelSight sensors have been used for several insertion tasks such as peg-in-hole [10], [16], [19], cable manipulation [12], USB insertion [22], and box-packing [23]. One work considers a dense optical-flow based feedback, which is decomposed into components of motion [24], and used for geometric reasoning about peg-hole relative position. In contrast our strain-like measurements are estimated from a homography based optical-flow estimator and its four corner representation is used without decomposition. Unlike any of these existing works we propose a model-free approach to solve the tactile insertion task.

III. METHODS

The algorithm has three parts. First, we describe the tactile feedback using strain measurements taken by a GelSight Mini tactile sensor and computed using a Lucas-Kanade style homography tracker. Next, we detail the objective function minimized by the extremum seeking control. Finally, we describe the extremum seeking control law, which sinusoidally perturbs the 6 degree of freedom pose of the end-effector

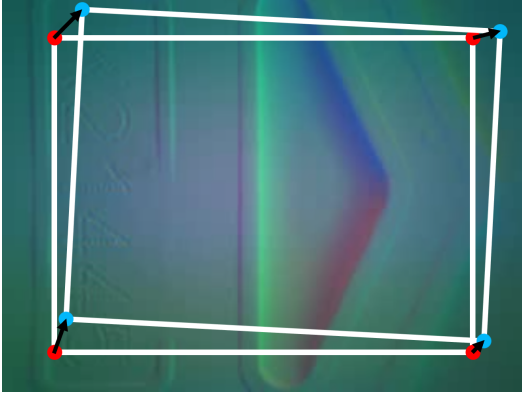


Fig. 3: A strain-like measurement is measured directly from the images returned by the GelSight Mini sensor. Each incoming frame is iteratively registered with a Lucas-Kanade style homography estimator to the first frame. The tracked patch has 10% margins with respect to the full frame and is exemplified by the area within the white box with red corners. The Euclidian norm of the corner displacements in pixels from their original location is used as the strain-like quantity L_{strain} .

to estimate a descent direction and minimize the objective function. A block diagram is given in Figure 2.

A. Tactile Strain Measurement

The gripper configuration is shown in Figure 1. Two GelSight Mini tactile sensors are pressed against the left and right side of the key head. One tactile sensor is off and functions as a soft barrier. The second sensor is on, and the 2D imagery captured from the internal camera is exemplified in Figure 3. Because the GelSight Mini contact pads are compliant, when pressure is applied to the tip of the key, the key moves with respect to the gel pads and warps the 2D imagery. Further, because the head of key is flat, this warp is described as an 8-parameter homography. Thus, a Lucas-Kanade style homography estimator is used to continuously warp back the current image to the first frame. The optimization is warm-started at each iteration using the previously estimated homography. The implementation is based on [25] and uses the 4 corner parameterization suggested in [26]. Before passing through the tracker, frames are resized to 320×240 resolution. The tracked patch is also initialized to the entire frame with 10% margins, as illustrated in Figure 3.

The displacement of the four corners of the tracked patch from its original position is used as the strain metric. That is

$$L_{strain}(t) = \sqrt{\sum_{i=1}^4 \|p_i(t) - p_i(t_0)\|^2}, \quad (1)$$

where $p_i(t)$ is the pixel location of the i 'th corner at time t as estimated by the homography tracker and t_0 is the time of the first frame. To avoid the effects of noise when pressure is

low $L_{strain} < 3$ pixels is reported as 0. The strain feedback is computed at 10-16 Hz. The update rate is limited by a combination of OpenCV's Python V4L2 camera interface, USB 2.0 bandwidth limits, and GelSight Mini's hardware requirement that images be retrieved at the high resolution of 3280×2464 in Motion-JPEG format.

B. Control Objective

To encourage the extremum seeking control to guide the key into the lock, an additional loss term $L_{insertion}$ is defined as

$$L_{insertion} = |Y - (Y(t_0) - d)|, \quad (2)$$

where Y is the position of the tip of the key in meters along the axis to be inserted into the lock, as illustrated by Figure 1. d is the depth of the keyhole. In order to force the algorithm to terminate, if $L_{insertion} < 0.5$ millimeters, the algorithm is stopped and insertion is considered a success.

The final objective function is then

$$L = L_{insertion} + \lambda L_{strain}, \quad (3)$$

where $\lambda = 0.0005$.

C. Extremum Seeking Control

Classical extremum seeking control as described in [3] is applied directly. A block diagram is given in Figure 2. The estimated parameters $\hat{\theta}$ are the 6 degree-of-freedom pose of the tip of the key. That is $\hat{\theta} = [X, Y, Z, \alpha, \beta, \gamma]^T$ where α, β, γ are $x - y - z$ intrinsic Euler angles corresponding to the orientation of the tip of the key.

As is standard in extremum seeking control. The instantaneously applied parameters $\theta(t)$ are modulated according to

$$\theta(t) = \hat{\theta}(t) + \text{diag}\{b\} \sin(wt), \quad (4)$$

Where b and w are vectors with the same dimensionality as θ , $\text{diag}\{\}$ is the operator that constructs a diagonal matrix from a vector, and \sin is applied element-wise. In all the experiments, $b_{1,2,3} = [0.2, 0.2, 0.5]^T$ millimeters, $b_{4,5,6} = [0.675, 0.675, 0.675]^T$ degrees and $w = [0.9, 0.83, 0.7, 1.05, 1.0, 0.95]^T$ Hz.

Following the standard extremum control pipeline, as illustrated by Figure 2, the objective L is sampled at each θ , resulting in a signal $L(t)$. $L(t)$ is high pass filtered with a first-order high pass filter with a 0.7 Hz cutoff, demodulated with $\sin(wt)$, and low pass filtered with a first-order filter with a cutoff of 1.59 Hz. This final signal is the feedback error multiplied by a control gain k to determine $\dot{\hat{\theta}}$. Precisely, the system that drives $\hat{\theta}$ is then

$$\dot{\hat{\theta}}(t) = -\text{diag}\{k\} \left[g_{lpf} * x_{demod} [g_{hpf} * L] \right](t). \quad (5)$$

Here $x_{demod}(t) = \text{diag}\{\sin(wt)\}$ is the demodulating signal, g_{lpf} is the impulse response of the low pass filter, g_{hpf} is the impulse response of the high pass filter, and $*$ denotes convolution. In the experiments $k = [0.7, 1.1, 0.7, 10.0, 10.0, 10.0]^T$. A UR10 robot arm was used to achieve the current θ using linear tool-space servoing.

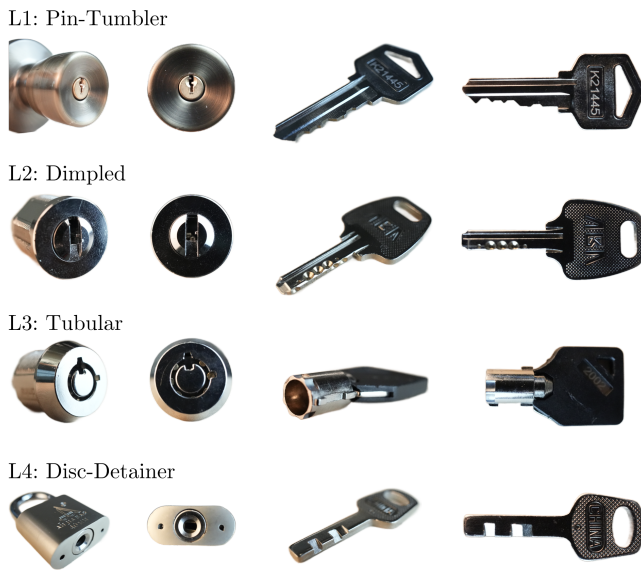


Fig. 4: The four types of key and lock pairs tested in experiments. L1 is a common pin-tumbler lock used on front doors. L2 is a dimpled cam lock that uses pin-tumblers like L1, but they also press on the sides of the key into the dimples. L3 is a tubular lock with a circular shape that must be pressed into the lock’s circular opening. Finally L4 is a disc-detainer padlock that features a series of rotating discs inside the lock itself that must be aligned according to the cutouts on the key’s face.

IV. EXPERIMENTS AND RESULTS

Two sets of experiments were performed on four distinct lock types. The first experiment involved 240 trials, and the second 120, for a total of 360 trials. The first experiment tested the effect of perturbing a single parameter from an initial pose aligned with the lock entrance. The results demonstrate which types of perturbations the method is sensitive to. The second experiment tests the effects of randomly initialized poses with pose uncertainty in translation and rotation, thus testing the methods robustness to significant misalignment.

A. Lock Types

Four locks were tested and illustrated in Figure 4. The first lock is a cylindrical pin-tumbler lock, an inexpensive design available at most hardware stores in the United States and commonly used on front doors. The ridges on the top of the key actuate the pin tumblers inside the lock. The second is a dimpled key cam lock that uses dimples on the sides of the key to actuate pin-tumblers inside the lock. Compared to a standard pin-tumbler, dimpled keys require some variation in force to insert due to the way the pin-tumblers press into the dimples. The third lock is a tubular cam lock. As shown in Figure 4 the tubular key is circular instead of rectangular and thus has a significantly different form than the pin-tumbler and dimpled keys. Cam locks are

commonly used in low-security applications such as securing cabinet doors or lockers. Finally, the fourth lock is a padlock disk-detainer. Disc-detainer locks use rotating disks that must be aligned rotationally, which is substantially different from pin-tumbler’s and tubular locks that force something aside during a straight-on insertion.

The lock offsets, d , were set to 18 millimeters for the cylindrical pin-tumbler, 19 millimeters for the dimpled, and 7 millimeters for the tubular. During the experiments with perturbation on one axis, the disc-detainer used a 19 millimeter offset except for the last 30 trials which used a 14 millimeter offset. The experiment with randomly initialized poses also used a 14 millimeter offset. The difference change was necessary due to increasing damage to the gel pads as experiments were conducted.

B. Initial Pose Perturbed on One Axis

The first experiment demonstrates the robustness to perturbations along one translation or rotational axis of the initial key pose away from alignment with the lock’s keyhole. For each lock, translation perturbations of -2.5, -1.9, 1.9, and 2.5 millimeters were tested along the plane parallel to the lock surface. Additionally, initial rotation perturbations of -10, -5, 5, and 10 degrees were applied to each orientation axis individually. A 0-millimeter and 0-degree setting corresponds to a near-perfect alignment between the key and the lock. Three tests were performed per initial pose. 1.9 mm is the maximum translational perturbation that ensures the key is in a convex region near the keyhole of every lock. The results are given in Table I.

The success rate over the smaller perturbations (-1.9 and 1.9 mm in translation) and (-5 and 5 degrees in rotation) was 90.8% over 120 trials with a mean insertion time of 122 seconds. The success rate over the large perturbations (-2.5 and 2.5 mm in translation) and (-10 to 10 degrees in rotation) dropped to 76.7% over 120 trials with a mean insertion time of 171 seconds. The overall success rate over the 240 trials was 83.8% with a mean insertion time of 147 seconds.

Lock L4 (Disc-Detainer) was the easiest as only one trial failed, resulting in a 98% success rate overall with mean insertion times of 98 seconds. Lock L1, L2, and L3 achieved 93%, 77%, and 65% overall with mean insertion times of 169, 232, and 105 seconds respectively. The drop in performance on lock L2 is expected because the lock features a small region of convexity around the keyhole, which makes it difficult for the extremum seeking control to enter the keyhole. Similarly, lock L3 is flat on the surface of the keyhole and so it proved difficult for the extremum seeking control to find the hole, especially when the perturbations were large.

C. Initial Pose Determined Randomly

Robustness to random initial poses was tested by drawing 30 random samples of end-effector pose. Translations on the plane parallel to the lock surface were drawn from a uniform distribution over -2.5 to 2.5 mm, and rotations in Euler angles were drawn from a uniform distribution over

Type of Lock	Translation Misalignment (mm)								Rotation Misalignment (deg)											
	X				Z				X				Y				Z			
	-2.5	-1.9	1.9	2.5	-2.5	-1.9	1.9	2.5	-10	-5	5	10	-10	-5	5	10	-10	-5	5	10
Success Rate (%)																				
L1	100	100	100	100	100	100	100	0	100	100	100	100	100	100	100	33	100	100	100	100
L2	67	67	100	0	33	100	33	67	100	100	100	67	100	100	100	100	67	100	67	67
L3	100	100	100	0	0	100	100	0	100	67	100	100	0	100	33	0	100	33	67	100
L4	100	100	100	100	100	100	100	100	100	100	100	67	100	100	100	100	100	100	100	100
Insertion Time (sec)																				
L1	322	96	93	117	215	106	93	-	232	116	113	217	505	91	85	120	160	123	136	181
L2	335	195	164	-	256	196	739	338	188	153	153	185	201	308	147	203	300	164	170	490
L3	335	89	83	-	-	118	53	-	145	36	80	155	-	44	62	-	85	41	52	106
L4	86	90	97	88	104	95	106	86	100	100	104	99	111	91	90	68	115	113	108	96

TABLE I: Success rate and insertion time versus single parameter perturbations of initial pose.

Type of Lock	Translation Misalignment (mm)								Rotation Misalignment (deg)											
	X				Z				X				Y				Z			
	(-2.5,-1.9)	(-1.9,0)	(0,1.9)	(1.9,2.5)	(-2.5,-1.9)	(-1.9,0)	(0,1.9)	(1.9,2.5)	(-10,-5)	(-5,0)	(0,5)	(5,10)	(-10,-5)	(-5,0)	(0,5)	(5,10)	(-10,-5)	(-5,0)	(0,5)	(5,10)
Success Rate (%)																				
L1	100	67	73	100	0	90	85	60	100	62	78	60	67	67	91	71	100	100	67	29
L2	50	67	80	0	100	80	54	40	62	62	78	40	67	67	64	57	70	43	67	71
L3	50	56	47	0	0	50	46	40	62	12	33	80	33	67	36	43	70	14	67	14
L4	100	100	100	100	100	100	100	100	100	100	100	100	100	100	100	100	100	100	100	100
Insertion Time (sec)																				
L1	125	277	204	169	-	226	177	285	205	261	173	225	173	161	270	449	151	161	167	383
L2	1360	387	429	-	545	416	385	860	389	430	594	289	303	571	507	594	346	556	410	587
L3	210	301	406	-	-	325	341	445	277	342	403	406	406	250	324	170	487	320	262	419
L4	135	130	138	125	132	107	139	173	114	109	123	223	165	103	150	106	106	146	129	153

TABLE II: Marginal distributions of success and insertion time when initial pose is random.

-10 to 10 degrees. The marginal distributions over the X, Z translation and X, Y, Z rotational axis are given in Table II.

The expected success rate over the uniformly sampled smaller translation perturbations (-1.9 to 1.9 mm) was 74% in X and 75% in Z with mean insertion times of 269 and 240 seconds respectively. Over the smaller rotational perturbations (-5 to 5 degrees), the expected success rate was 66% in X, 73% in Y (insertion direction), and 69% in Z with mean insertion times of 274, 241, and 253 seconds respectively. The success rate over larger translation perturbations (-2.5 to 2.5 mm) was 58% in X and 57% in Z with mean insertion times of 233 and 355 seconds respectively. Over the larger rotational perturbations (-10 to 10 degrees), the expected success rate was 77% in X, 67% in Y (insertion direction), and 72% in Z with mean insertion times of 247, 291, and 268 seconds respectively.

The overall success rate was 71% over 120 trials with a mean insertion time of 262 seconds.

As in the preceding experiment, Lock L4 (Disc-Detainer) was the easiest, with zero failures and a mean insertion time of 134 seconds. Lock L1, L2, and L3 achieved 77%, 63%, and 44% overall and mean insertion times of 210, 465, 351 seconds respectively over the 30 randomly initialized trials.

V. DISCUSSION AND FUTURE WORK

The potential of a model-free wiggling based approach to key-in-lock insertion, that generalizes without changes to multiple types of locks, has been demonstrated. Our approach achieves high success rates on two out of four locks (L1 and L4). In particular, L4 achieved a very high success rate due to

its smooth and relatively convex lock face over the range of perturbations tested. The other two locks (L2 and L3) achieve markedly lower success rates, this is expected due to the limitations of the straightforward application of Extremum Seeking Control. Further, it can be seen from the significant differences in average insertion times between these two groups of locks that the formulation's main difficulty is finding the lock opening on locks with non-convex faces. This is entirely expected because extremum seeking only works on convex problems and in general a more sophisticated search procedure is needed for finding the keyhole.

The other reasons for failure are summarized per lock. Lock L1 (pin-tumbler) has sharp edges along the top and bottom of the key hole that the key can become stuck in. In this case, our method is too naive to detect that the key is stuck, or wedged, and thus does not back away (12 failure cases). Lock L2 (dimpled) had sharp edges on the key that sometimes became caught on the entrance of the lock, resulting in a similar failure mode as L1 (7 failure cases). Additionally, L2 has a raised keyhole as can be seen in Figure 4. Thus, it was common for the extremum seeking control law to move the key over the edge of this raised region and get stuck in the local minima (11 failure cases). Finally, lock L3 (tubular) achieved the lowest success rate because of the circular design of L3's key. In this case, correct orientation about the Y axis (insertion axis) is much more important than in L1, L2, or L4. Additionally, the surface of the lock is flat, and thus provides little to no information for the extremum seeking control law to use to proceed into the lock (33 failure cases). These two issues also occasionally caused

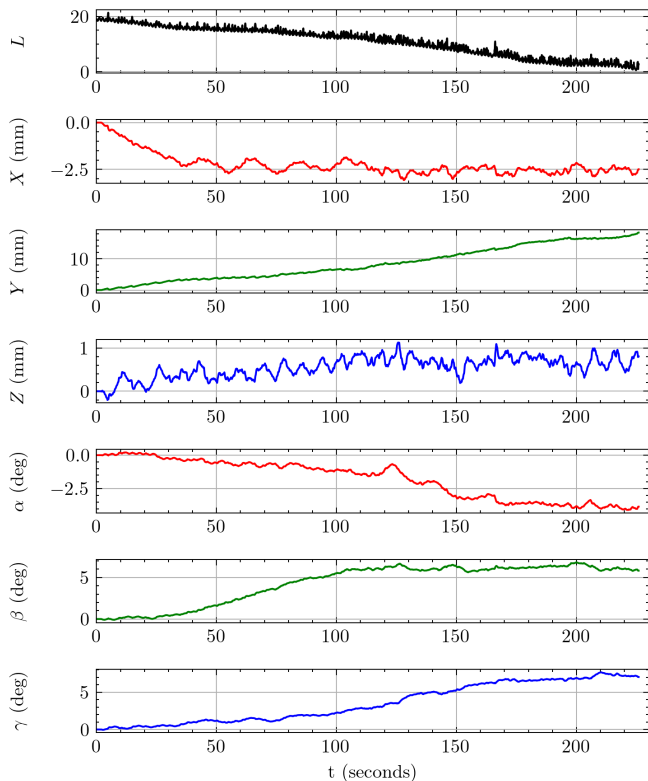


Fig. 5: The loss and estimated parameters (end-effector pose) converge as the key is inserted. The Y parameter increases steadily because it corresponds to the insertion axis. The trial pictured was initialized with $[1.1, 0.0]$ millimeters of translation along the X, Z axis and $[3.4, -7.4, 5.7]$ degrees of rotation about the X, Y, Z axis. The discrepancy between initial the translation offsets and converged to parameter estimates are due to the clearance of the key and keyhole.

a maximum limit on strain to be exceeded (3 failure cases). The reasons for five cases of failure were not recorded.

It is clear that most of these failures are due to limitations of the direct application of extremum seeking control to a problem that is not convex. However, there are many ways to improve. The most straightforward is to augment the objective to include information such as the expected location of the keyhole and known geometry of the lock (either measured with 3D sensors, or recalled with a prior) in the objective function. Further, machine learning based approaches may prove useful for augmenting the cost function especially, when dealing with more complex contact dynamics. Finally, machine learning can be used to augment the extremum seeking control policy directly. For example, the extremum seeking perturbations do not need to be sinusoidal and task-specific periodic perturbations could be learned instead.

The current approach also admits several immediate paths towards improving the mean insertion time and success rate. In particular, the control parameters were tuned only to demonstrate efficacy and not for robustness to random initial pose or minimization of insertion times. Additionally, the

objective function is currently linear in each argument and thus results in slow, linear convergence as seen in Figure 5. It should be possible to simply reshape the objective function in order to greatly improve insertion times. Similarly, a modeled prior such as the relative independence of axis motion on the strain-like measurement could allow faster convergence and robustness. Finally, the current system’s compliance is determined solely by the gripper’s gel pads. Thus, future work can consider impedance control to both enhance the sense of strain and improve compliance during insertion.

Because Extremum Seeking Control is a form of optimization, it is reasonable to ask what other types of optimizers could be used instead. Extremum Seeking Control is a form of zero-order optimization that is suited for mechanical systems. There exist other algorithms for zero-order optimization, however most focus on estimating the gradient of the objective through finite-differencing, which naively results in discontinuous motions [27]. In contrast, Extremum Seeking Control also estimates a gradient like quantity from smooth perturbations and as such many extensions exist with the goal of achieving properties commonly achieved in traditional optimization algorithms such as second order convergence [3].

Type	Examples	Tactile Modalities
Direct	Key, Seatbelt	Grasp strain
Through	Cable routing Putting on belt	Grasp strain Bimanual contact
Crowded	Putting a cup in a cupboard Packing a box	Grasp strain Manipulator contact

TABLE III: Classification of insertion problems where humans employ wiggling-based strategies. Direct insertion is studied in this paper through the process of key insertion. The study of through and crowded insertion problems are proposed as future work.

As a broad source of future work, we propose a generalization of wiggling-based tactile insertion. Table III enumerates three categories of insertion (direct, through, and crowded), with application examples and tactile modalities that must be accounted for. Direct insertion considers problems such as key insertion or latching a seatbelt. In these cases, a wiggling-based insertion strategy can use the strain measured by a tactile sensor. Similarly, through insertion, which considers problems such as routing cables through holes or putting a belt, relies on grasp strain but also typically requires tactile feedback from passing the inserted object from one hand to the other. Finally, in crowded insertion, where a manipulator places a cup in a cupboard or packs a box, grasping strain and skin-like contact between the manipulator and the already placed objects becomes essential.

ACKNOWLEDGMENTS

The authors thank Antonio Gambale for helpful discussions about lock types and characteristics. The support of the NSF under award OISE 2020624 is gratefully acknowledged.

REFERENCES

- [1] W. Yuan, S. Dong, and E. H. Adelson, "GelSight: High-resolution robot tactile sensors for estimating geometry and force," *Sensors*, vol. 17, no. 12, 2017.
- [2] M. Leblanc, "Sur l'électrification des chemins de fer au moyen de courants alternatifs de fréquence élevée," *Revue générale de l'électricité*, vol. 12, no. 8, pp. 275–277, 1922.
- [3] A. Scheinker, "100 years of extremum seeking: A survey," *Automatica*, vol. 161, p. 111481, 2024.
- [4] C. Yan, J. Wu, and Q. Zhu, "Learning-based contact status recognition for peg-in-hole assembly," in *2021 IEEE/RSJ International Conference on Intelligent Robots and Systems (IROS)*, 2021, pp. 6003–6009.
- [5] S. Chhatpar and M. Branicky, "Localization for robotic assemblies using probing and particle filtering," in *Proceedings, 2005 IEEE/ASME International Conference on Advanced Intelligent Mechatronics*, 2005, pp. 1379–1384.
- [6] H. Park, J. Park, D.-H. Lee, J.-H. Park, M.-H. Baeg, and J.-H. Bae, "Compliance-based robotic peg-in-hole assembly strategy without force feedback," *IEEE Transactions on Industrial Electronics*, vol. 64, no. 8, pp. 6299–6309, 2017.
- [7] H. Park, J. Park, D.-H. Lee, J.-H. Park, and J.-H. Bae, "Compliant peg-in-hole assembly using partial spiral force trajectory with tilted peg posture," *IEEE Robotics and Automation Letters*, vol. 5, no. 3, pp. 4447–4454, 2020.
- [8] S. Gubbi, S. Kolathaya, and B. Amrutur, "Imitation learning for high precision peg-in-hole tasks," in *2020 6th International Conference on Control, Automation and Robotics (ICCAR)*, 2020, pp. 368–372.
- [9] B. Calli, W. Caarls, M. Wisse, and P. P. Jonker, "Active vision via extremum seeking for robots in unstructured environments: Applications in object recognition and manipulation," *IEEE Transactions on Automation Science and Engineering*, vol. 15, no. 4, pp. 1810–1822, 2018.
- [10] S. Kim and A. Rodriguez, "Active extrinsic contact sensing: Application to general peg-in-hole insertion," in *2022 International Conference on Robotics and Automation (ICRA)*, 2022, pp. 10241–10247.
- [11] O. Gibbons, A. Albini, and P. Maiolino, "A tactile feedback insertion strategy for peg-in-hole tasks," in *2023 IEEE International Conference on Robotics and Automation (ICRA)*, 2023, pp. 10415–10421.
- [12] Y. She, S. Wang, S. Dong, N. Sunil, A. Rodriguez, and E. Adelson, "Cable manipulation with a tactile-reactive gripper," *The International Journal of Robotics Research*, vol. 40, no. 12-14, pp. 1385–1401, 2021.
- [13] R. J. Chang, C. Lin, and P. Lin, "Visual-based automation of peg-in-hole microassembly process," *Journal of Manufacturing Science and Engineering*, vol. 133, p. 041015, 08 2011.
- [14] S. Liu, D. Xu, F. Liu, D. Zhang, and Z. Zhang, "Relative pose estimation for alignment of long cylindrical components based on microscopic vision," *IEEE/ASME Transactions on Mechatronics*, vol. 21, no. 3, pp. 1388–1398, 2016.
- [15] H. Lee, S. Park, K. Jang, S. Kim, and J. Park, "Contact state estimation for peg-in-hole assembly using gaussian mixture model," *IEEE Robotics and Automation Letters*, vol. 7, no. 2, pp. 3349–3356, 2022.
- [16] T. Kamijo, I. G. Ramirez-Alpizar, E. Coronado, and G. Venture, "Tactile-based active inference for force-controlled peg-in-hole insertions," 2023. [Online]. Available: <https://arxiv.org/abs/2309.15681>
- [17] K. Nottensteiner, F. Stulp, and A. Albu-Schäffer, "Robust, locally guided peg-in-hole using impedance-controlled robots," in *2020 IEEE International Conference on Robotics and Automation (ICRA)*, 2020, pp. 5771–5777.
- [18] K. Zhang, M. Shi, J. Xu, F. Liu, and K. Chen, "Force control for a rigid dual peg-in-hole assembly," *Assembly Automation*, vol. 37, pp. 200–207, 04 2017.
- [19] S. Dong, D. K. Jha, D. Romeres, S. Kim, D. Nikovski, and A. Rodriguez, "Tactile-RL for insertion: Generalization to objects of unknown geometry," in *2021 IEEE International Conference on Robotics and Automation (ICRA)*, 2021, pp. 6437–6443.
- [20] H. Lin, R. Corcodel, and D. Zhao, "Generalize by touching: Tactile ensemble skill transfer for robotic furniture assembly," 2024. [Online]. Available: <https://arxiv.org/abs/2404.17684>
- [21] N. Fukaya, K. Yamane, S. Masuda, A. Ummadisingu, S. ichi Maeda, and K. Takahashi, "Four-axis adaptive fingers hand for object insertion: FAAF hand," 2024. [Online]. Available: <https://arxiv.org/abs/2407.21245>
- [22] R. Li, R. Platt, W. Yuan, A. Ten Pas, N. Roscup, M. A. Srinivasan, and E. Adelson, "Localization and manipulation of small parts using gelsight tactile sensing," in *2014 IEEE/RSJ International Conference on Intelligent Robots and Systems*. IEEE, 2014, pp. 3988–3993.
- [23] S. Dong and A. Rodriguez, "Tactile-based insertion for dense box-packing," in *2019 IEEE/RSJ International Conference on Intelligent Robots and Systems (IROS)*. IEEE, 2019, pp. 7953–7960.
- [24] G. Wang, X. Liu, Z. Liu, P. Huang, and Y. Yang, "Visual-tactile perception based control strategy for complex robot peg-in-hole process via topological and geometric reasoning," *IEEE Robotics and Automation Letters*, vol. 9, no. 10, pp. 8410–8417, 2024.
- [25] S. Baker and I. Matthews, "Lucas-Kanade 20 years on: A unifying framework," *International Journal of Computer Vision*, vol. 56, no. 3, pp. 221–255, 2004.
- [26] S. Baker, A. Datta, and T. Kanade, "Parameterizing homographies," Pittsburgh, PA, Tech. Rep. CMU-RI-TR-06-11, March 2006.
- [27] S. Liu, P.-Y. Chen, B. Kailkhura, G. Zhang, A. O. Hero III, and P. K. Varshney, "A primer on zeroth-order optimization in signal processing and machine learning: Principals, recent advances, and applications," *IEEE Signal Processing Magazine*, vol. 37, no. 5, pp. 43–54, 2020.